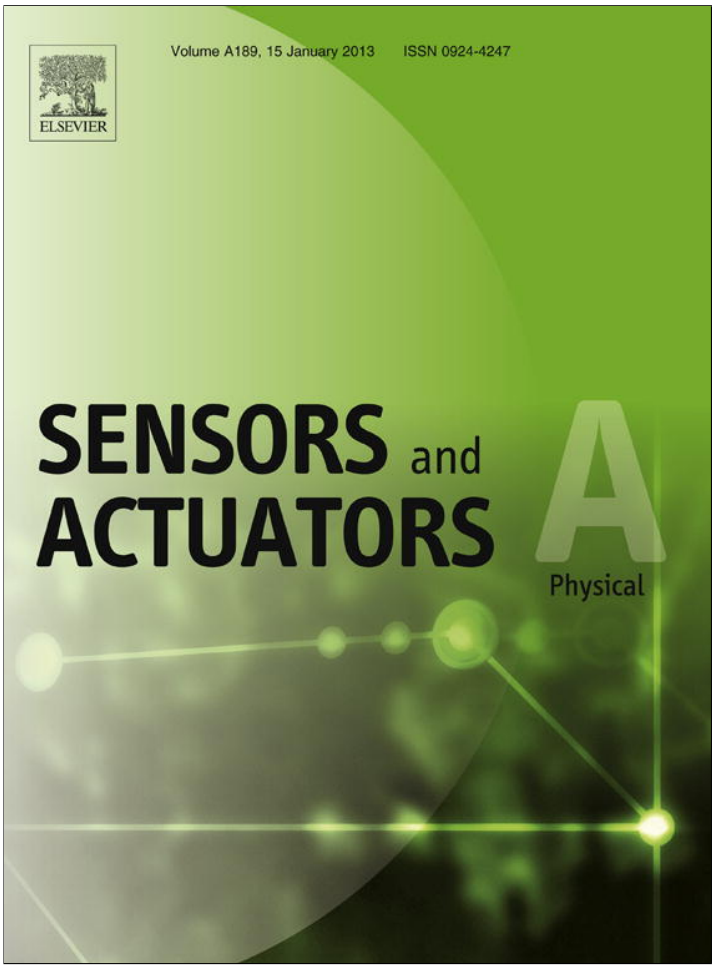

Sensors and Actuators A 189 (2013) 238–253

Contents lists available at SciVerse ScienceDirect

Sensors and Actuators A: Physical

journal homepage: www.elsevier.com/locate/sna

Doppler-tolerant receiver for an ultrasonic LPS based on Kasami sequences

Fernando J. Álvarez[a,*], Álvaro Hernández[b], José A. Moreno[a], M. Carmen Pérez[b], Jesús Ureña[b], Carlos De Marziani[c]

[a] Department of Electrical Engineering, Electronics and Automatics, University of Extremadura, E-06071 Badajoz, Spain
[b] Electronics Department, University of Alcalá, E-28806 Alcalá de Henares, Spain
[c] National University of Patagonia San Juan Bosco and CONICET, Ciudad Universitaria, Ruta Prov. 1, Km. 4, 9005 Comodoro Rivadavia, Chubut, Argentina

ARTICLE INFO

Article history:
Received 20 March 2012
Received in revised form 8 September 2012
Accepted 27 September 2012
Available online 16 October 2012

Keywords:
LPS
Doppler-tolerance
Kasami sequences
Field-Programmable Gate Array (FPGA)

ABSTRACT

This paper presents the design of a novel receiver for a broadband ultrasonic Local Positioning System (LPS). As in other devices based on matched filtering of the transmitted encoded signals, this receiver features high robustness to noise and multiple access capability. Unlike previous solutions, the proposed receiver is capable of detecting beacons emissions despite being installed in a fast moving device, and it also provides estimation of its velocity. The system has been implemented in an FPGA-based architecture. An experimental analysis of performance has been carried out. Firstly using a set of test signals synthetically generated to simulate different positions and velocities of the receiver. Secondly, a set of real signals obtained with a prototype have been used. The simulated results show the capability of the system to detect the encoded signals emitted by the LPS infrastructure when the device is moving at velocities of up to 3 m/s under low SNR conditions. The real results confirm the improved system capability, but also make evident the negative influence that phenomena such as the transducers response and multipath propagation can have on system performance.

1. Introduction

Intelligent Environments (IEs) have been subject of increasing research activity for the last two decades. Generally speaking, they can be defined as interactive spaces with embedded computers and sensors that use context information to seamlessly enhance ordinary activity. One of the most important elements of context is user location and thus, Local Positioning Systems (LPS) have evolved in parallel with other basic components of IEs. Many systems based on various technologies have been proposed to date, including ultrasonic [1–7], radio-frequency [8–10], optical [11,12] and magnetic [13]. There is a general agreement that the main advantages of ultrasonic systems are their relatively low cost and their high resolution, the latter being a direct consequence of the low speed of sound in air.

During the first years of the past decade some ultrasonic LPS (uLPS) were proposed that achieved centimetric resolution through the emission of ultrasonic pulses. These uLPS could be centralized, where the object to be located acts as the emitter [1], or privacy-oriented, where this object is in charge of computing its own position using the signals received from different beacons [2]. The use of narrowband signals made these systems very susceptible to noise, though, and also, the update rate was very limited due to the necessity of avoiding signal collisions.

Shortly after, signal coding was incorporated into these systems. For this purpose families of binary codes with good correlation properties were chosen. The use of Direct Sequence Spread Spectrum (DSSS) techniques brought important advantages such as robustness to noise, multiple access capability (allowing increased update rates) and higher resolution. One of the first broadband systems was proposed by Hazas and Ward, who used Gold sequences in the design of both centralized [3] and privacy-oriented [4] uLPSs. Since then, several works based on DSSS have arisen that employ more efficient encoding schemes, using Kasami [5] or Loosely Synchronous (LS) [6] codes. Also, Frequency Hopping Spread Spectrum (FHSS) techniques have been recently used as an alternative to DSSS apparently improving the accuracy of these systems under conditions of noise and reverberation [7].

However, the low speed of sound in air that allows high-resolution positioning is also the cause of a new difficulty in broadband systems. Some authors have pointed out that the Doppler shift, caused by the user movement in the ultrasonic encoded signal, could make it completely unrecognizable to the receiver [14,15]. This is a well-known problem in radar theory whose effects are considerably more pronounced in acoustic systems, since the ratio between the speed of the receiver/reflector

* Corresponding author. Tel.: +34 924 28 93 00; fax: +34 924 28 95 43
E-mail addresses: fafranco@unex.es (F.J. Álvarez), alvaro@depeca.uah.es (Á. Hernández), josan@unex.es (J.A. Moreno), carmen@depeca.uah.es (M.C. Pérez), urena@depeca.uah.es (J. Ureña), marziani@unpata.edu.ar (C. De Marziani).

0924-4247/$ – see front matter © 2012 Elsevier B.V. All rights reserved.
http://dx.doi.org/10.1016/j.sna.2012.09.029

and the propagation speed of the signal is typically several orders of magnitude larger than in radar. As an example, this ratio would be $(3.43 \times 10^3)/(3 \times 10^8) = 1.14 \times 10^{-5}$ in a radar station tracking one of the fastest aircraft (the unmanned NASA X-43), whereas it would increase to $1.8/343 = 5.25 \times 10^{-3}$ in a uLPS tracking a walking person.

Recent work has analysed the effect of Doppler shift on pulse compression of ultrasonic signals encoded with different families of binary codes [16]. This work has experimentally demonstrated that Kasami sequences are one of the most robust solutions against this shift. It has shown that radial user speeds as low as 1.5 m/s can drastically deteriorate the auto-correlation properties of a 255-bit Kasami sequence, BPSK modulated with one cycle of a 50 kHz carrier. This limit is even lower for other encoding schemes based on Complementary Sets of Sequences or Loosely Synchronized Codes.

This paper presents the design of a Doppler-tolerant receiver for a broadband uLPS architecture based on the emission of 255-bit Kasami codes. Previous work has proposed the simultaneous estimation of a receiver's position and velocity from a set of independent ultrasonic beacons [17,18]. These works make use of low-power wireless ultrasonic beacons that emit ultrasonic pulses with a regular periodicity of around 500 ms. Both the position and the velocity of the receiver are estimated by iteratively measuring the Doppler shift in the transmission period using a Kalman [17] or a particle [18] filter. However, as stated before, the narrowband nature of these emissions leads to coarse position accuracies of about 25 cm. Also, the estimated receiver's velocity is actually an average over a transmission period and unfortunately the authors do not provide quantitative data on velocity estimation accuracy.

To the authors' knowledge, the receiver presented in this work is the first real-time system than can calculate the time of arrival of the signals emitted by a broadband uLPS and simultaneously estimate its own velocity. The rest of the paper is organized as follows: Section 2 describes in detail the uLPS architecture, the main features of Kasami codes, and the effect that the user movement can have on the detection of these codes by pulse compression. In Section 3, the global structure of the proposed receiver is presented. Hardware implementation in a FPGA-based architecture is later described in detail in Section 4. The performance of this system is statistically analysed in Section 5 by using both synthetic and real signals. The main conclusions drawn from this work are finally outlined in Section 6.

2. Global description of the uLPS

2.1. LPS architecture

The LPS whose receiver is proposed in this work is inspired by Global Positioning System (GPS). A set of beacons are placed at known positions of an environment where a non-limited number of portable receivers can compute their position in an independent and autonomous way. These beacons are wired synchronized and perform simultaneous and periodic emission of signal patterns that are asynchronously detected by the receiver. The receiver is capable of computing its absolute position from the Differences in Time-of-Arrival (DTOA) between a reference beacon and the others by means of a hyperbolic trilateration algorithm. Unlike GPS, based on spherical trilateration, there is no need for a common time base or synchronizing signal between the beacons and the receivers in this system.

Fig. 1(a) shows a schematic representation of the LPS architecture, where the spatial distribution of the five beacons comprising this architecture can be observed. At every location, the receiver must be capable of detecting the signals coming from at least three beacons to compute its 2D location in a horizontal plane of known height. Four beacons are necessary to perform 3D positioning, and an additional beacon can be used to eliminate the speed of sound from the set of positioning equations, thus avoiding the need to measure room temperature. These beacons are deployed over a metallic 1 m × 1 m structure placed on the ceiling at 3.45 m high, with the distribution shown in Fig. 1(b).

Every beacon is composed of a Polyvinylidene Flouride (PVDF) ultrasonic transducer with a maximum response frequency at 40 kHz and 8 kHz bandwidth, inserted into a conic reflector designed to enlarge the coverage area [19]. These transducers are driven by a power stage that amplifies the emission patterns generated by a Spartan3E FPGA [20], from the binary sequences and modulation symbol previously stored in its RAM memory blocks. This device is connected via USB to a PC from where different features of the emissions, such as the carrier frequency or the time between firings, can be configured.

2.2. Signal coding and detection

As stated before, all beacons in the LPS perform their emissions simultaneously and, to diminish the effect of Multiple-Access-Interference (MAI), a set of emissions with low cross-correlation values must be chosen. Various families of binary codes with this property have been already proposed in the design of these systems, such as Gold sequences, Kasami sequences, Complementary Set of Sequences and LS codes. Nevertheless, recent work has demonstrated that not all of these codes are equally resilient to the Doppler shift caused by receiver movement [16], and proposes the use of Kasami sequences as a compromise between their fairly good correlation properties obtained with a stationary receiver and the reduced deterioration of these properties with increasing receiver velocity.

Kasami sequences [21] belong to the well-known family of Pseudo Noise (PN) sequences, that are generated using linear feedback shift-registers and exclusive OR-gate circuits. A new Kasami sequence $c[n]$ can be obtained from a maximal sequence and the decimated and concatenated version of this sequence by performing the module-2 sum of the former with any delayed version of the latter, i.e.,

$$c = m_1 \oplus D^l m_2 \quad \text{with } l < L \tag{1}$$

where m_1 is a maximal sequence of length $L = 2^{N-1}$ with N even; m_2 is the sequence obtained from the decimation of m_1 with a decimation factor of $q = 2^{N/2} + 1$ and the concatenation of the result q times; $\oplus$ represents the module-2 sum; and $D^l m_2$ is the sequence obtained by cyclically shifting the m_2 sequence l positions. A family of sixteen 255-bit sequences ($N = 8$) has been generated following this procedure, and from them, a set of $I = 5$ sequences with optimal correlation properties has been chosen as the sequences for the proposed uLPS.

The chosen binary codes are BPSK (Binary Phase Shift Keying) modulated in order to adapt the spectrum of the emission to the frequency response of the ultrasonic transducer. This modulation scheme has been widely used to transmit binary codes in matched filtering-based sonar systems [22,23]. Every bit in the code $c[n]$ is modulated with one or more carrier cycles whose phase, 0 or π, is given by the bit value to obtain the modulated pattern $p[n]$ as:

$$p[n] = \sum_{i=0}^{L-1} c[i] \cdot s[n - i \cdot M] \tag{2}$$

where L is the code length; $s[n]$ is the modulation symbol; and M represents the number of samples in this symbol, given by the product between the number of carrier cycles composing this symbol and the ratio between the sampling and the carrier frequencies, f_S and f_c respectively.

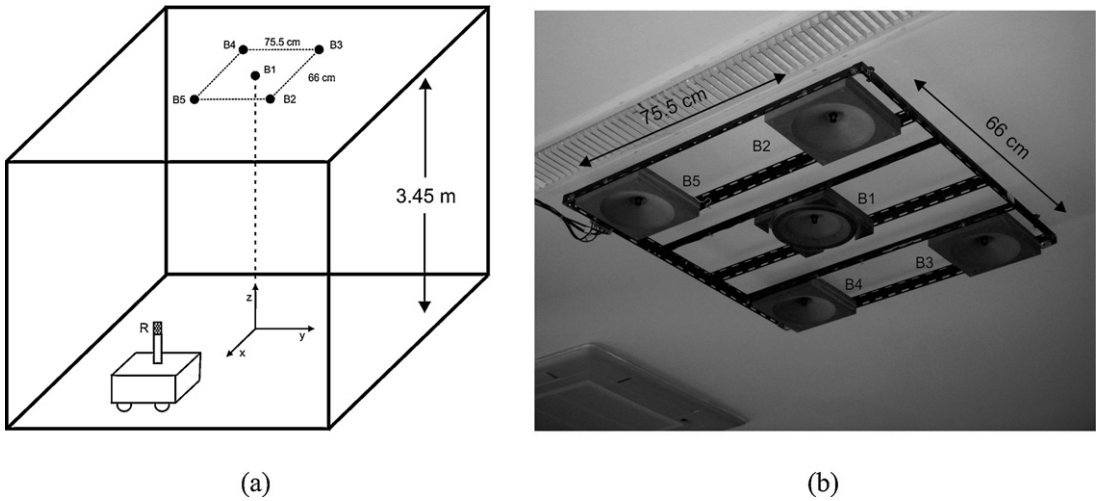

Fig. 1. LPS architecture: (a) schematic representation and (b) picture of the actual beacons structure.

A simple receiver for this LPS architecture would be composed of an ultrasonic transducer/microphone, an amplifier, an A/D converter, a demodulation stage, a bank of five Kasami correlators (KC), one matched to each beacon emission, and a bank of five peak detectors to search for the maxima above a threshold in the correlator outputs. The temporal occurrences of these peaks are sent to a local computer where the DTOAs are computed and the positioning algorithm evaluated. As an example, Fig. 2 shows the signals obtained at the output of the bank of five KCs when the receiver is at position $\mathbf{r} = (1, 1, 1)$ m and the signal-to-noise ratio (SNR) is equal to 0dB. As shown in Fig. 1(a), the origin of the coordinates is assumed to be at the vertical projection over the floor of the central beacon.

2.3. Effect of receiver movement on signal detection

The system described above has been proven to work reliably over a rectangular surface of 4.5 m × 3.5 m, with the receiver (a mobile robot) moving at velocities below 0.2 m/s. However, as

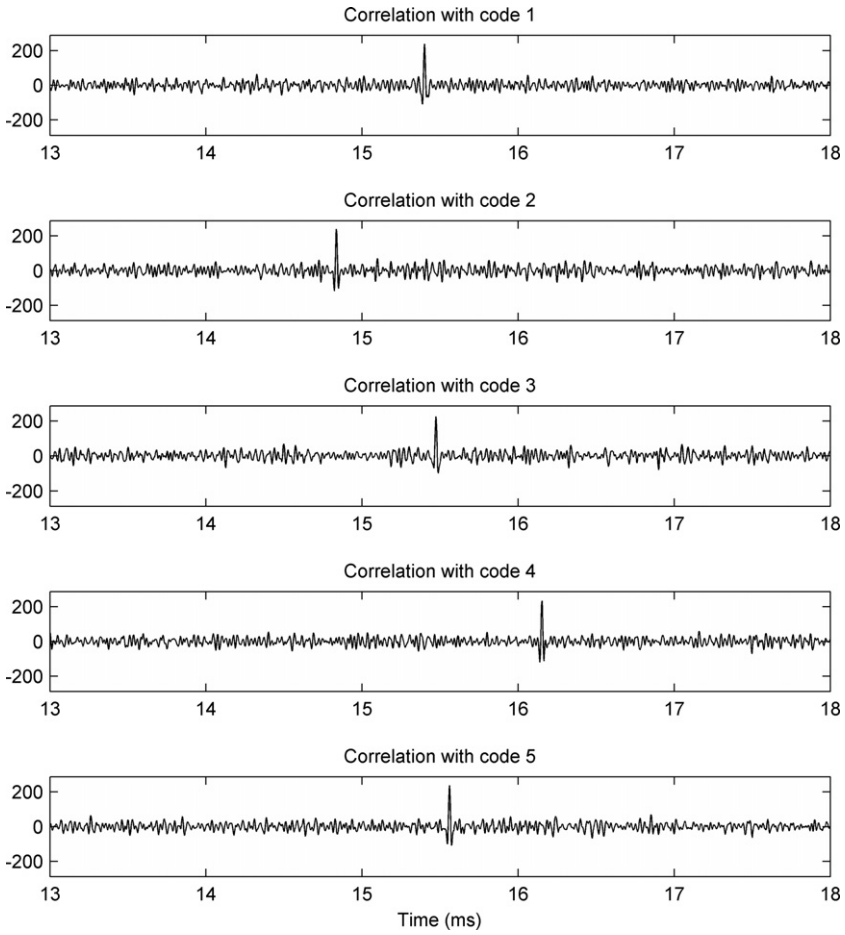

Fig. 2. Signals obtained at the output of the KCs bank for a receiver at position $\mathbf{r} = (1, 1, 1)$m for five beacons (B1, B2, . . ., B5) and SNR = 0 dB.

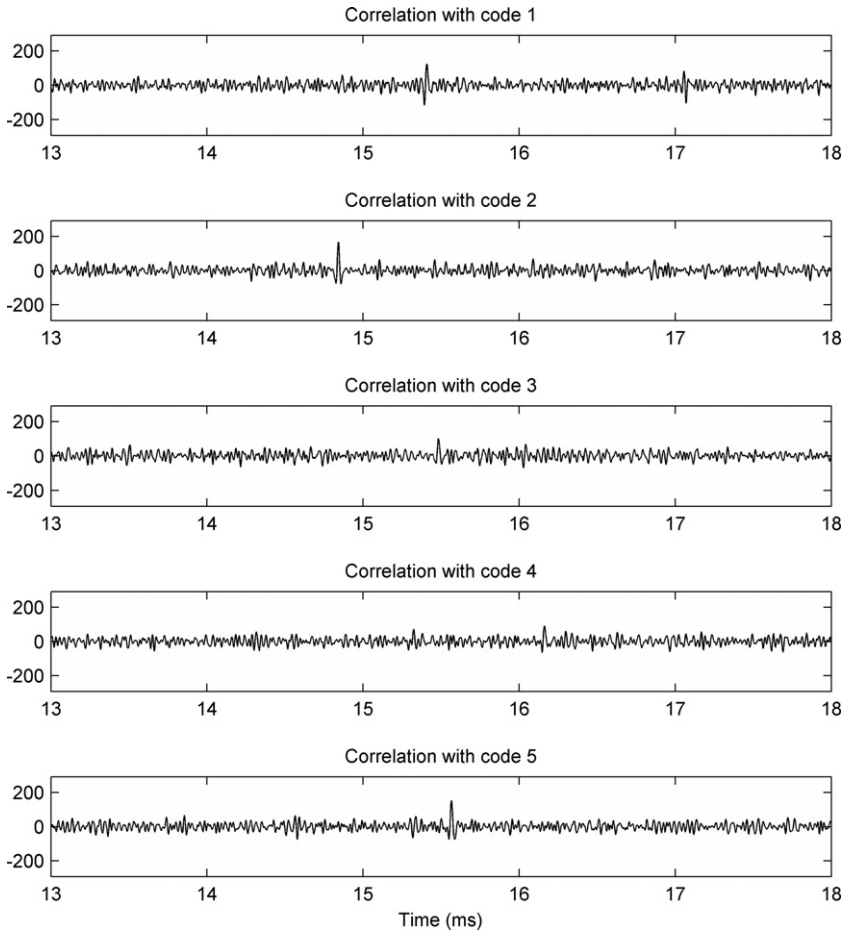

Fig. 3. Signals obtained at the output of the KCs bank for a receiver at position $\mathbf{r} = (1, 1, 1)$ m and velocity vector $\mathbf{v} = (3, 0, 0)$ m/s (SNR = 0 dB).

stated in Section 1, larger velocities could make the received signals completely unrecognizable to the matched filters due to Doppler shift. Fig. 3 shows the same situation as represented in Fig. 2, but with the receiver moving with a velocity vector of $\mathbf{v} = (3, 0, 0)$ m/s. As can be observed, most of the AC peaks appear severely reduced, and might not be detected regardless of using a low value for the detection threshold.

This phenomenon can be characterized by means of the auto- and cross-correlation bounds of a family of K modulated codes, defined as:

$$\theta_{AC} = \max\left\{\frac{\phi_{r_i p_i}[k]\,\forall k \notin [-G\cdot M, G\cdot M]}{\max \phi_{r_i p_i}} \quad \forall i \in \{1, \ldots, K\}\right\} \tag{3a}$$

$$\theta_{CC} = \max\left\{\frac{\phi_{r_i p_j}[k]\,\forall k}{\max \phi_{r_i p_i}} \quad \forall i, j \in \{1, \ldots, K\}, \quad i \neq j\right\} \tag{3b}$$

where $\phi_{rp}[n]$ is the aperiodic correlation function between the received signal $r[n]$ and the stored pattern $p[n]$; M is again the number of samples in the modulation symbol; and G is a guard factor that avoids the effect of the large sidelobes obtained in the vicinity of the main peak ($G = 3$ in this work). The representation of the auto-correlation bound against the receiver radial velocity causing the Doppler shift of the received signal s_i shows the difficulty to detect a code by matched filtering with a moving receiver. Equivalently, the representation of the cross-correlation bound against this velocity gives an idea of how the reception of a Doppler-shifted code makes the detection of other codes in the family difficult.

Fig. 4 shows experimental data for θ_{AC} and θ_{CC} obtained with the help of an electric slider that accurately controls the velocity of the ultrasonic receiver up to a maximum of 2 m/s. As can be seen, the cross-correlation bound of this family of five 255-bit Kasami sequences remains close to a relatively constant value of 0.2 regardless of the receiver velocity, what means that the reception of a Doppler-shifted code always has a similar effect on the detection of another code of the family. This is not true for other families of binary codes, as described in detail in [16]. With respect to the auto-correlation bound, this parameter rapidly increases with increasing receiver radial velocity, as expected and reported in previous works. Depending on the application and the signal processing carried out to detect the auto-correlation peaks, values of this parameter above 0.5 could not be admissible, which determines the maximum receiver radial velocity of about 1 m/s in this system.

3. Doppler tolerant receiver

If fast moving receivers ($v > 1$ m/s) wanted to make use of the uLPS infrastructure described in the previous section, one simple and straightforward solution would be to use a bank of matched filters instead of a single filter to demodulate every encoded emission. These filters must be matched to the discrete-time Doppler-shifted versions of the modulated symbol received at different radial velocities, with a maximum increment of $\Delta v_{max} = 2$ m/s between consecutive filters in the bank for this velocity. This simple approach is represented in Fig. 5(a).

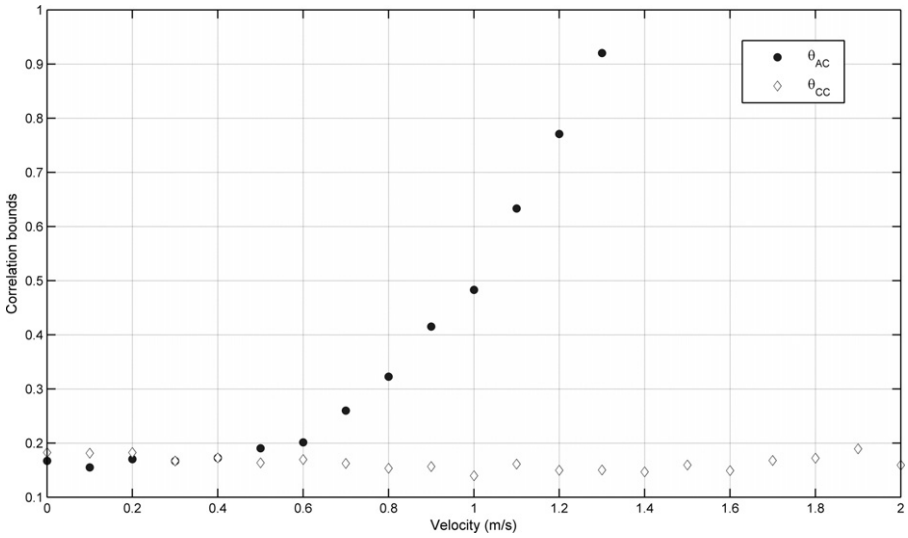

Fig. 4. Experimental data for the auto- and cross-correlation bounds of the family of modulated Kasami codes as a function of the receiver velocity. Values of θ_{AC} beyond 1.3 m/s are not defined because at these velocities the main peak of the auto-correlation function is no longer in the vicinity of the zero-delay point.

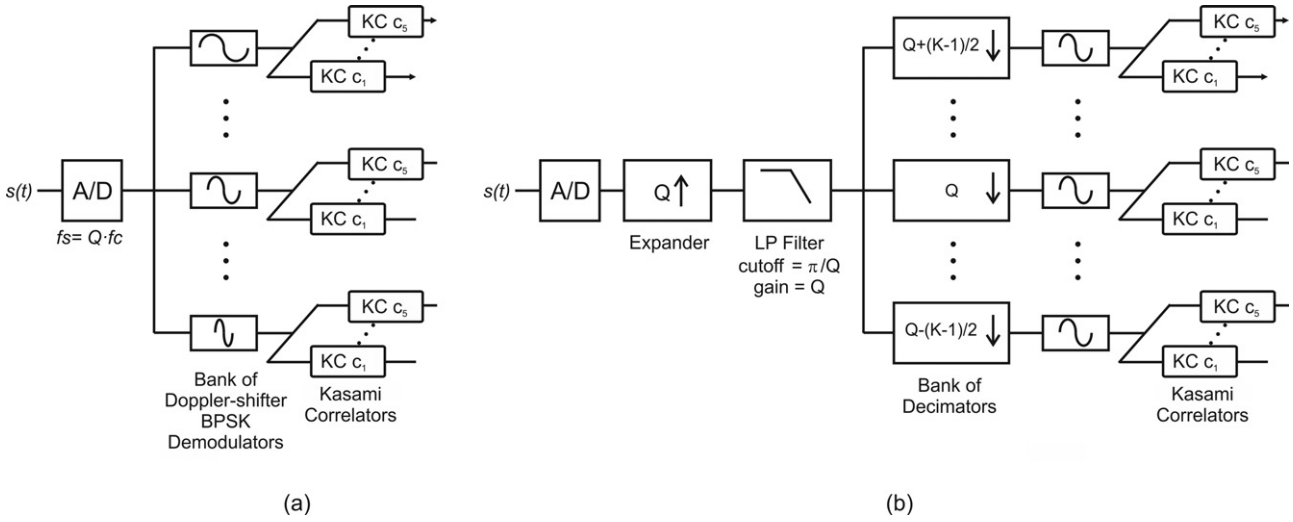

Fig. 5. Two different approaches for the core stage of the Doppler-tolerant receiver. (a) Bank of filters matched to the Doppler-shifted modulation symbols and (b) multirate filter bank.

In this work, we propose the design of a Doppler-tolerant receiver based on a bank of $K=7$ matched filters for every code c_i to be detected, giving a total of $I \times K = 5 \times 7 = 35$ filters for all the five beacons. These filters are matched to the ideal signal that would reach the receiver when moving with radial speeds of $n \cdot \Delta v_r$ m/s, with $n \in \{0, \pm 1, \pm 2, \pm 3\}$ and a velocity resolution $\Delta v_r = 0.67$ m/s. This value is considerably smaller than the maximum value of 2 m/s established above, what will allow a more accurate estimation of the receiver speed at the expense of reducing its maximum admissible value. The absolute value for this limit will become in the proposed system $3 \times 0.67 + 1 \approx 3$ m/s, which is large enough to locate persons and/or medium-speed mobile robots.

However, for this approach to work, the sampling frequency f_S of the A/D converter must be high enough as to provide an integer number of samples in every Doppler-shifted modulation symbol. Otherwise, the matched filtering could not be performed in the two stages process represented in Fig. 5(a), a configuration that notably reduces the resources needed in the hardware implementation of the system. Taking into account that the period of the Doppler-shifted carrier can be expressed as:

$$T_c'(v_r) = T_c \cdot \frac{c}{c + v_r} \tag{4}$$

where T_c is the period of the non-shifted carrier; c is the speed of sound; and v_r is the radial speed of the receiver, the latter condition can be expressed as:

$$T_c'(v_{r_k}) = \left(Q + \frac{K+1}{2} - k\right) \cdot T_S \quad \text{with} \quad k = [1, 2, \ldots, K] \tag{5}$$

where T_S is the sampling period; $Q = f_S/f_c$ is the ratio between the sampling frequency and the non-shifted carrier frequency; K is the number of demodulators; and v_{r_k} is the receiver radial speed the demodulator k is matched to, v_{r_1} and v_{r_K} being the maximum negative and positive velocities respectively. By combining Eqs. (4) and (5), and taking into account that $T_c = Q \cdot T_S$, we have,

$$Q \cdot T_S \frac{c}{c + v_{r_k}} = \left(Q + \frac{K+1}{2} - k\right) \cdot T_S \tag{6}$$

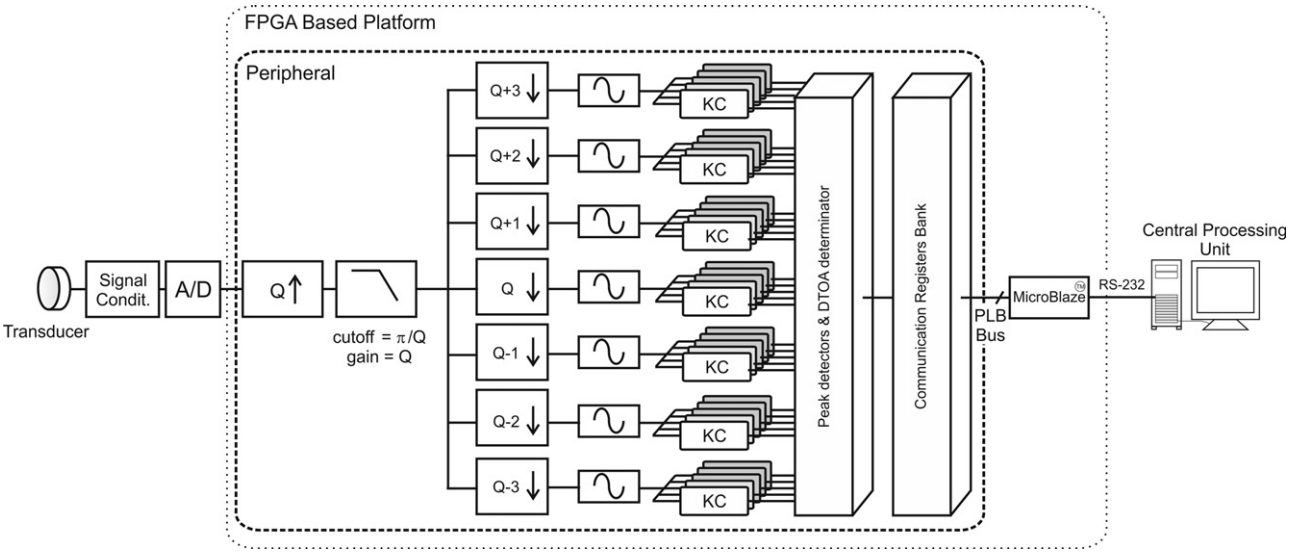

Fig. 6. Block diagram of the Doppler-tolerant receiver.

This, after some manipulation yields:

$$Q = \left(k - \frac{K+1}{2}\right) \cdot \frac{c + v_{r_k}}{v_{r_k}} \tag{7}$$

If, as expected in our system, $|v_{r_k}| << c \quad \forall k$, then Eq. (7) can be further simplified as:

$$Q \approx \left(k - \frac{K+1}{2}\right) \frac{c}{v_{r_k}} \tag{8}$$

Or, equivalently, we can write for the radial speed:

$$v_{r_k} \approx \left(k - \frac{K+1}{2}\right) \frac{c}{Q} = \left(k - \frac{K+1}{2}\right) \Delta v_r \tag{9}$$

where $\Delta v_r = c/Q$ is the Doppler resolution, i.e., the increment of receiver radial velocity between two consecutive demodulators. Eq. (8) can be finally expressed in terms of the Doppler resolution as,

$$Q \approx \frac{c}{\Delta v_r} \tag{10}$$

This relation states that a factor of $Q = 512$ is necessary to obtain the desired Doppler resolution of about 0.67 m/s. This value implies a sampling frequency f_S $Q = 512$ times greater than the carrier frequency f_c, and an internal operation frequency f_{mclk} in the Kasami correlators $L = 255$ times greater than this sampling frequency f_S for a real-time implementation. As a carrier frequency $f_c = 39.0625$ kHz was chosen for the ultrasonic emissions of the LPS, an internal operation frequency f_{mclk} about 5.1 GHz would be required in this approach, which is not an achievable frequency in a FPGA-based solution.

An alternative approach to that explained above consists in using a multirate filter bank to compensate for the Doppler shift caused by the receiver's movement, following the scheme shown in Fig. 5(b). Let assume that the received signal $r(t)$ is sampled at f_S, thus giving the discrete-time signal $r[n]$ with spectrum $R(e^{j\omega})$. This signal is first expanded by a factor of Q by including $Q-1$ zeroes between consecutive samples of $r[n]$. A new signal $r_i[n] = r[n/Q]$ for $n = 0, \pm Q, \pm 2Q, \ldots$ and 0 otherwise, is thus obtained whose spectrum $R_i(e^{j\omega})$ is a Q-fold compressed version of $R(e^{j\omega})$, i.e.,

$$R_i(e^{j\omega}) = R(e^{j\omega Q}) \tag{11}$$

As shown in Fig. 5(b), the expanded signal $r_i[n]$ is next filtered by a low-pass (LP) filter whose transfer function is given by,

$$H_{LP}(e^{j\omega}) = \begin{cases} Q & 0 \le |\omega| \le \pi/Q \\ 0 & \text{otherwise} \end{cases} \tag{12}$$

to obtain a new signal $r_f[n]$ with spectrum $R_f(e^{j\omega})$ given by,

$$R_f(e^{j\omega}) = \begin{cases} Q \cdot R(e^{j\omega Q}) & 0 \le |\omega| \le \pi/Q \\ 0 & \text{otherwise} \end{cases} \tag{13}$$

This signal is then fed into a bank of K decimators with decimation factor of $Q - k + (K+1)/2$, for $k = [1, 2, \ldots, K]$, from where K signals $r_{d,k}[n] = r_f[n \cdot (Q - k + (K+1)/2)]$ are obtained. Assuming the absence of aliasing, the spectra $R_{d,k}(e^{j\omega})$ of these signals are given by:

$$R_{d,k}(e^{j\omega}) = \frac{Q}{Q - k + (K+1)/2} R(e^{j\omega(Q/(Q+(K+1)/2-k))})$$
$$0 \le |\omega| \le \pi \quad k = [1, 2, \ldots, K] \tag{14}$$

If the received signal $r(t)$ has been emitted as the pattern $p(t)$ by a certain beacon, and the receiver is moving towards this beacon with speed v_{r_k}, the spectra of the discrete-time versions of these signals $r[n]$ and $p[n]$ are related as:

$$R(e^{j\omega}) = P(e^{j\omega(c/(c+v_{r_k}))}) \tag{15}$$

where c is again the speed of sound. Combining Eqs. (14) and (15) the spectra of the signals coming out from the decimators can finally be expressed as:

$$R_{d,k}(e^{j\omega}) = cte \cdot R(e^{j\omega(Q/(Q+(K+1)/2-k))})$$
$$= cte \cdot P(e^{j\omega(Q/(Q+(K+1)/2-k))(c/c+v_{r_k})}) \tag{16}$$

From this expression, it is clear that the frequency shift caused by the receiver's movement is cancelled if,

$$\frac{Q}{Q + (K+1)/2 - k} \frac{c}{c + v_{r_k}} = 1 \tag{17}$$

which is identical to Eq. (6) derived before, that yielded Eqs. (7) and (10) when $|v_{r_k}| \ll c \; \forall k$. To obtain a Doppler resolution of about 0.67 m/s, an expansion factor of $Q = 512$ is thus needed.

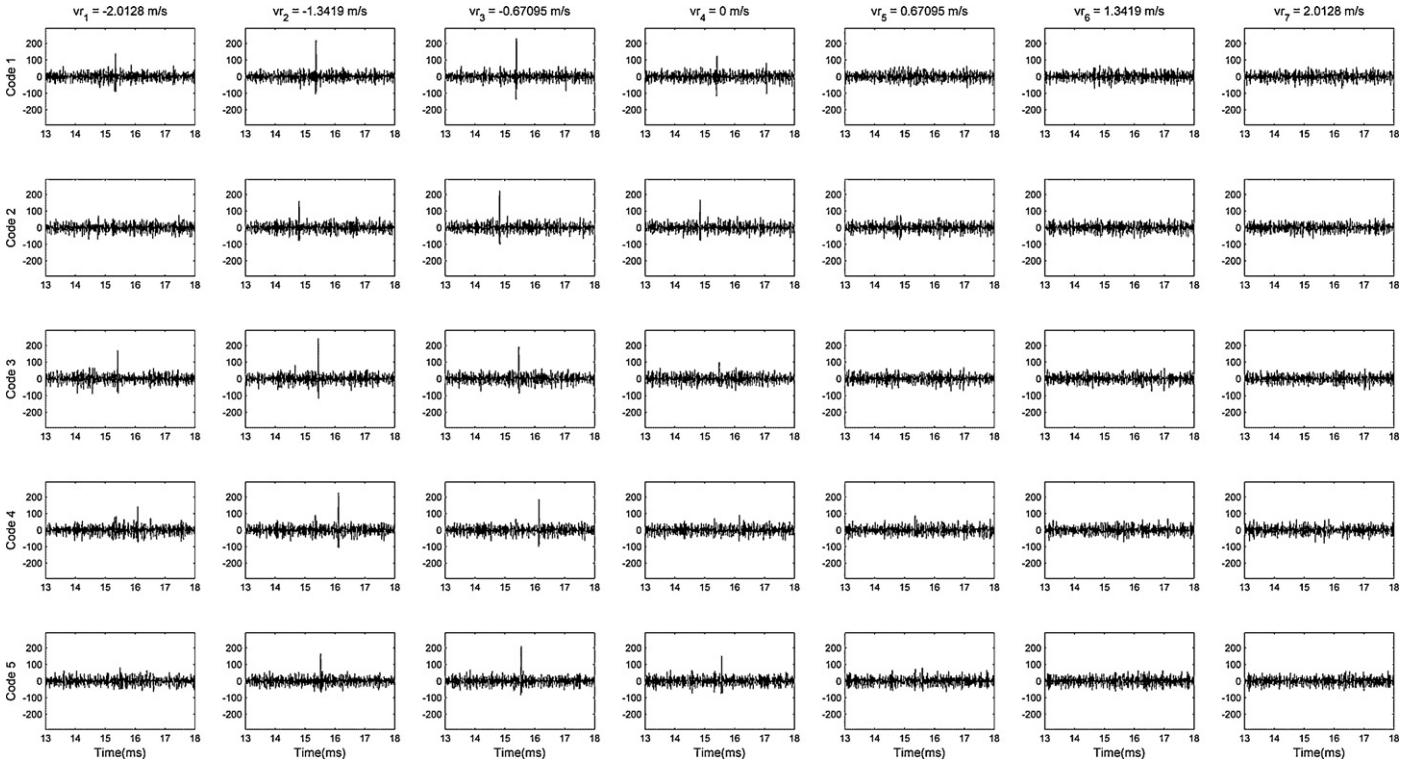

Fig. 7. Signals obtained at the outputs of the KCs in the proposed Doppler-tolerant receiver. The receiver is placed at position $\mathbf{r}=(1, 1, 1)$ m with velocity vector $\mathbf{v}=(3, 0, 0)$ m/s (SNR = 0 dB).

Fig. 6 shows the block diagram of the whole Doppler-tolerant receiver based on the multirate filter bank for $K=7$. In addition to this core stage, the diagram also includes the high-level processing modules described next.

As can be seen in this figure, the KCs outputs are fed into a peak detection and DTOAs determination stage, whose threshold is adjusted to determine 35 pairs ($DTOA_{k,i}$, $PM_{k,i}$, $k=[1, 2, \ldots, 7]$, $i=[1, 2, \ldots, 5]$) in every firing cycle, where $DTOA_{k,i}$ is the Differential Time-Of-Arrival of the peak obtained at the output of the correlator matched to radial speed v_{r_k} and code c_i, and $PM_{k,i}$ is the magnitude of this peak. This information is stored in a bank of communication registers that, together with all the stages described above, constitute a complex peripheral that will be accessed by a Microblaze processor via PLB bus. This soft-core processor performs three tasks:

- Obtains the DTOA of code c_i as the DTOA for the peak with the highest amplitude obtained among the $K=7$ correlators matched to this code.
- Estimates the radial speed v_i of the receiver with respect to beacon i as a weighted average of the reference velocities, using as weights the magnitude of the peaks $PM_{k,i}$ obtained in the correlators:

$$v_i = \frac{\sum_{k=1}^{7} PM_{k,i} v_{r_k}}{\sum_{k=1}^{7} PM_{k,i}} \tag{18}$$

- Communicates these results via serial port to a central computer to visualize them and to determine the receiver location from the hyperbolic trilateration algorithms.

Fig. 7 shows an example of the signals obtained at the output of the KC modules of this receiver in the scenario represented in Fig. 3, with a receiver at position $\mathbf{r}=(1, 1, 1)$ m moving with a velocity vector $\mathbf{v}=(3, 0, 0)$ m/s. The central column in this figure represents the output of the correlators matched to the non-shifted signal, and must provide identical results than those represented in Fig. 3. The first, second and third columns represent the outputs of the correlators matched to receiver radial speeds of −2.01 m/s, −1.34 m/s and −0.67 m/s respectively, whereas the fifth, sixth and seventh columns represent the output of the correlators matched to receiver radial speeds of 0.67 m/s, 1.34 m/s and 2.01 m/s respectively. As can be seen, the system is capable of detecting correlation peaks in all rows, i.e., all codes are detected. Moreover, the largest peaks are obtained in the third column for codes c_1, c_2 and c_5, and in the second column for codes c_3 and c_4. This means that the receiver radial speeds with respect to beacons B1 to B5 are close to −0.67 m/s, −0.67 m/s, −1.34 m/s, −1.34 m/s and −0.67 m/s respectively. The actual radial speeds can be easily calculated from vectorial calculus, and turn out to be: −0.97 m/s, −0.69 m/s, −1.28 m/s, −1.19 m/s and −0.64 m/s for beacons B1 to B5 respectively. As mentioned before, these correlated signals are fed into a peak detection and DTOAs determination stage, that provides 35 pairs ($DTOA_{k,i}$, $PM_{k,i}$, $k=[1, 2, \ldots, 7]$, $i=[1, 2, \ldots, 5]$). In this example, the processor calculates DTOA values of 578, 0, 620, 1295 and 725 μs for codes c_1 to c_5 respectively, and estimates receiver radial speeds of −1.02, −0.65, −1.33, −1.28, and −0.45 m/s with respect to beacons B1 to B5 respectively.

4. Receiver implementation

4.1. Peripheral design

The complex peripheral described above has been implemented in a FPGA-based platform, following the schematic diagram depicted in Fig. 8. All the modules in this design have been suitably pipelined to achieve high enough data rates, with a master clock frequency f_{mclk} of 100 MHz, obtained from the external clock signal. In addition to this clock, $K=7$ Doppler enable signals (shown as $EnDoppler_k$ in Fig. 8) are generated to correctly synchronize the

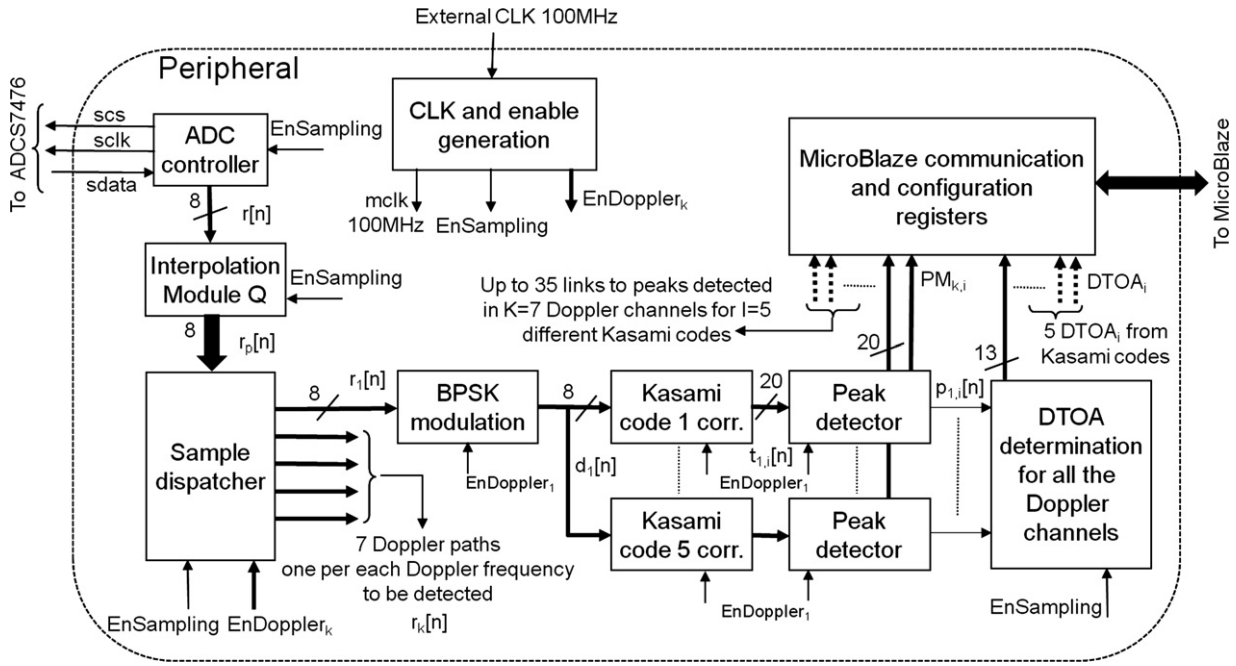

Fig. 8. Global block diagram of the peripheral implementation.

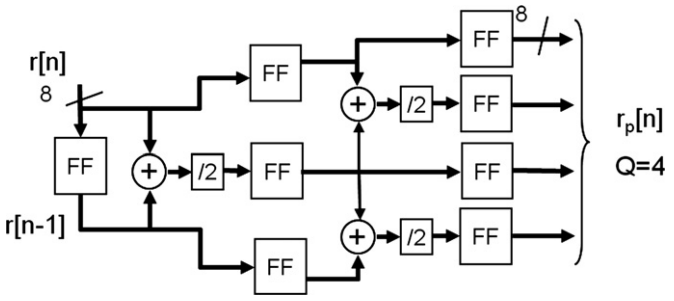

Fig. 9. Block diagram of the interpolation module with $Q = 4$.

operation at every k Doppler branch. Furthermore, the system processes a new sample every $T_{mclk} = 10$ ns and so, assuming an internal interpolation factor $Q = 512$, the sampling enable, noted as *EnSampling*, should be generated to drive the ADC controller and the interpolation block at a frequency $f_S = f_{mclk}/Q = 390.625$ kHz.

The received signal $r[n]$ is coming through an ADC controller, which is in charge of managing a SPI-type connection to the ADCS7476 device available in the hardware platform. The controller is configured to provide a new 8-bit sample every 1/390, 625 = 2.56 μs.

The expansor-LP filter pair following the A/D converter in Fig. 6 is implemented in practice as a linear interpolation module. The architecture of this module is fully pipelined, as shown in Fig. 9 for $Q = 4$ (the extension to $Q = 512$ is straightforward). The number of segments in the pipeline is equal to $\log_2 Q$. This allows high frequency of operation, but also implies a latency in the block of $\log_2 Q - 1$. This latency is not significant since the outputs are computed before the next sample $r[n]$ arrives at a frequency f_S. Note that this block requires the current sample $r[n]$, as well as the previous one $r[n-1]$. For this purpose, an initial flip–flop register (FF) is used. The datawidth is 8 bits at the input and at the output. Internal division by two is applied by shifting, and the least significant bit (LSB) is discarded to keep the same datawidth.

The interpolated signal $r_p[n]$ consists of $Q - 1$ new values between two consecutive samples $r[n]$ and $r[n-1]$. From that

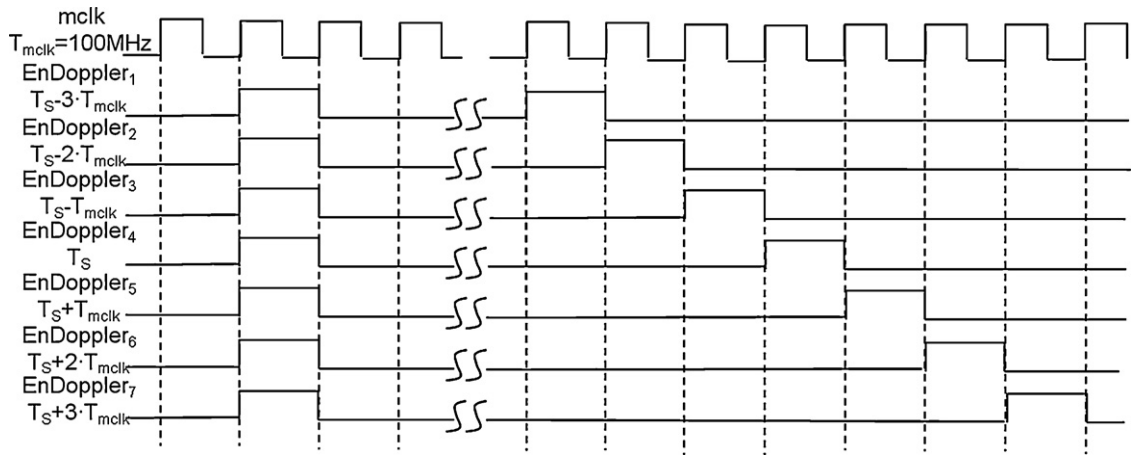

Fig. 10. Timing proposed for the Doppler enable signal $EnDoppler_k$.

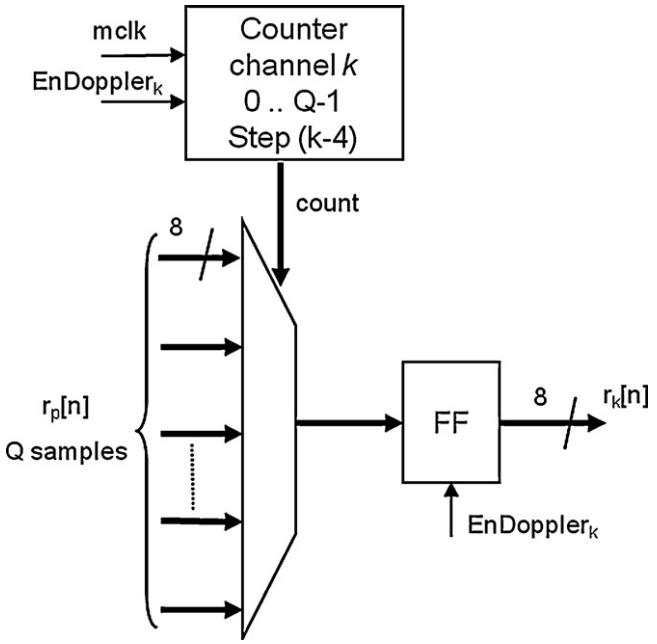

Fig. 11. Block diagram of the dispatch module for sampling frequency $f_{S,k}$.

moment, a different processing branch is arranged for each sampling frequency $f_{S,k}$. Each branch k has its own enable signal $EnDoppler_k$, and the input signal $r_k[n]$, with $k = [1, 2, 3, 4, 5, 6, 7]$, must be arranged by taking the suitable samples from the interpolated signal $r_p[n]$. Fig. 10 shows the timing for the Doppler enable $EnDoppler_k$. It is important to remark that the signal $EnDoppler_4$ corresponds to the sampling frequency f_S (*EnSampling*), associated with a static receiver. For other enable signals $EnDoppler_k$, with $k \neq 4$, frequencies are lower or higher, depending on the receiver's velocity direction.

The block in charge of providing the corresponding input signal $r_k[n]$ to each Doppler branch k is shown as *Sample dispatcher* in Fig. 8, and represents the practical implementation of the decimators bank appearing in Fig. 6. This block performs the multiplexing of the Q available samples from the interpolated signal $r_p[n]$, according to the value of a counter. The modulus of these counters is Q and the incremental step is $(k-4)$ for sampling frequencies $f_{S,k}$ with $k = [1, 2, 3, 4, 5, 6, 7]$. Fig. 11 shows the generic design of this module.

After that, every Doppler branch k consists of a BPSK demodulation, a correlation to seek the corresponding Kasami code c_i, and a peak detector to detect the arrival of transmissions coming from beacon i.

The BPSK demodulation is carried out in a sequential way, according to the scheme shown in Fig. 12. A buffer stores the last $M = f_S/f_c = 10$ samples which are multiplied by a carrier period $s[n]$ and accumulated, as indicated by Eq. (19). The samples of the carrier period $s[n]$ are stored in a ROM memory. This demodulation module has already been described in [5].

$$d_k[n] = \sum_{l=0}^{M-1} r_k[l+n] \cdot s[l] \tag{19}$$

The demodulated signal $d_k[n]$ is correlated with the Kasami codes c_i assigned to the $I = 5$ beacons available in the system according to (20), for $i = [1, 2, 3, 4, 5]$.

$$t_{k,i}[n] = \sum_{l=0}^{L-1} d_k[l \cdot M + n] \cdot c_i[l] \tag{20}$$

where $t_{k,i}$ is the correlation for sampling frequency $f_{S,k}$ and for Kasami code c_i; L is the length of the Kasami codes; and M is the oversampling factor $M = f_S/f_c = 10$.

Correlation is carried out according to a straightforward method based on two accumulators proposed in [24] (see Fig. 13). This allows a significant reduction in resource consumption, although the design is time constrained. In fact, L additions have to be computed for each new sample $d_k[n]$ every $T_{S,k}$. This implies a minimum value for the operation frequency f_{mclk} of the design, which allows

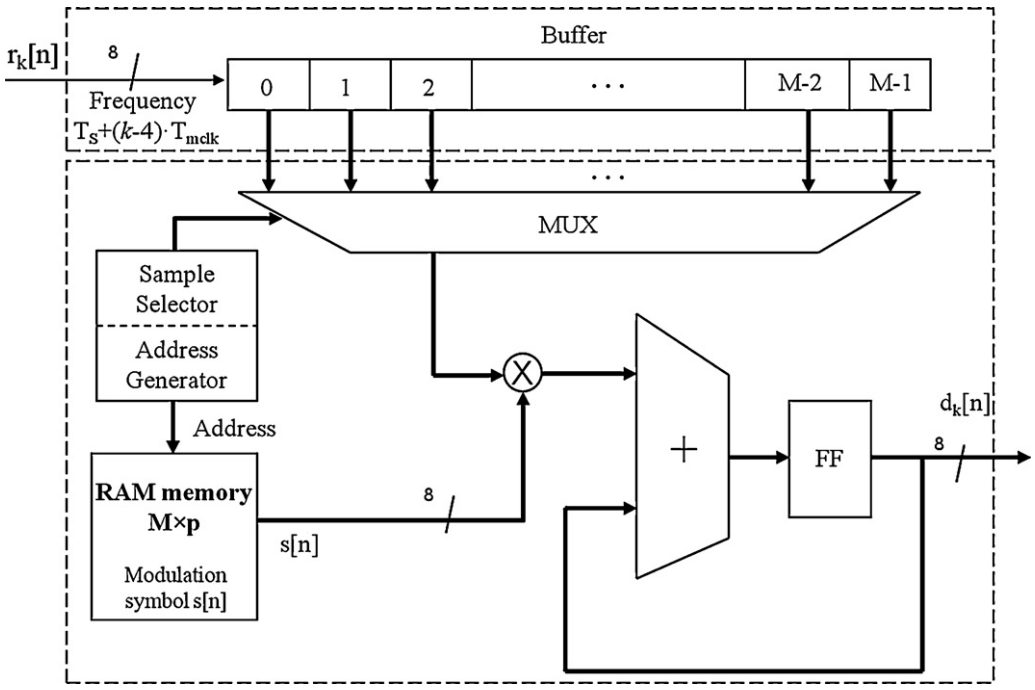

Fig. 12. Block diagram of the BPSK demodulation implementation.

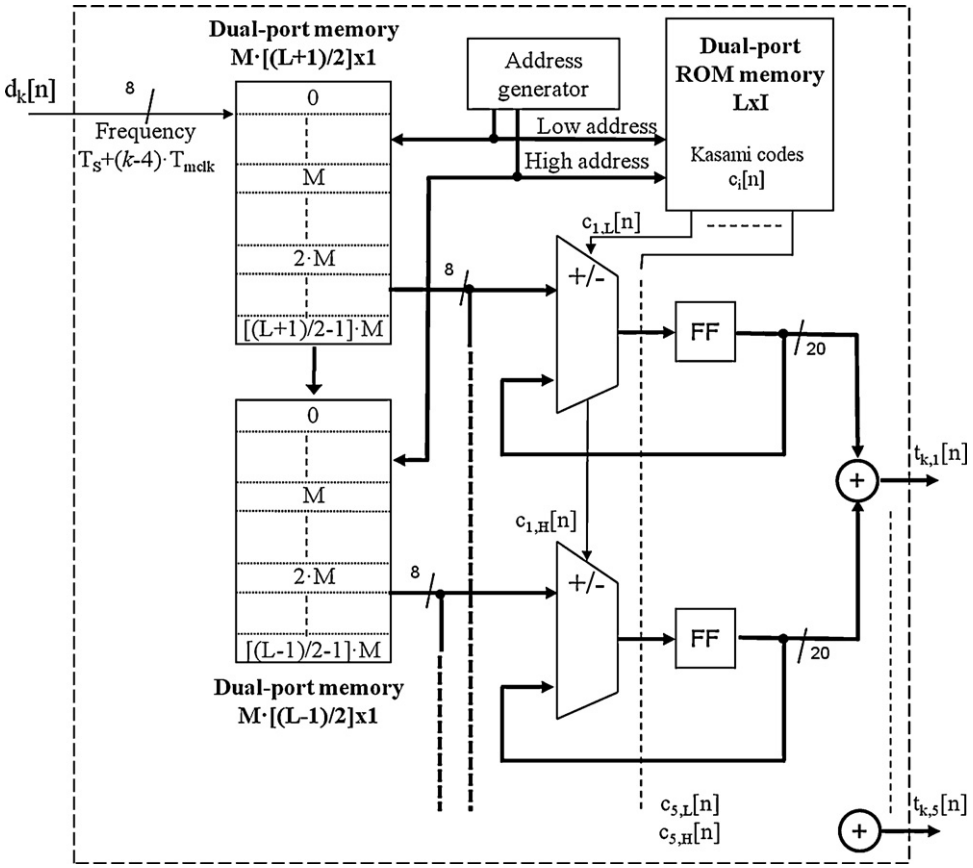

Fig. 13. Block diagram of the correlation implementation.

completion of the whole correlation process, given by the worst case $k = 7$:

$$f_{mclk} \geq \lceil \frac{L}{2} \rceil \cdot f_{S,7} = 128 \times 392,927.31\,\text{Hz} \approx 50.29\,\text{MHz} \quad (21)$$

Finally, the correlated signal $t_{k,i}[n]$ is analysed by a peak detector in order to detect and validate the maximum values as transmissions from the beacons in the output signal $p_{k,i}[n]$. As can be observed in Fig. 14, the signal $t_{k,i}[n]$ must be higher than a threshold $U_{k,i}$ to be considered as a possible peak, and it will be validated if there is no higher values inside the analysis window $W_{k,i}$. This module has been already described in [25].

The detection signals $p_{k,i}[n]$ are processed by the DTOA determination module in order to determine the differences in time $DTOA_{k,i}$ between the beacons at the different sampling frequencies $f_{S,k}$, as well as the maximum values $PM_{k,i}$ (see Fig. 15).

4.2. Microblaze processor

The final hardware design is based on a SoPC (System on a Programmable Chip) solution implemented in an FPGA. This kind of solution allows implementing a complete system composed of a microprocessor, controllers, IP modules and programmable logic for custom design in a single programmable device. This technology provides many advantages in terms of functionality, cost, board area and flexibility, and allows customization to add any combination of peripherals and controllers.

In this work, a Xilinx MicroBlaze soft-core processor has been used. The receiver core integration is done by a PLB bus (Processor Local Bus) in a memory-mapped mode addressing with 45 read/write internal registers, as well as an event controller which generates an interrupt for the microprocessor on new data arrival and processing. The Microblaze single-precision floating-point unit (FPU) can be used to estimate the radial speed v_i and the position of the receiver, by means of the differences in times of arrival $DTOA_{k,i}$ and the maximum values $PM_{k,i}$.

5. Experimental results

The full design has been implemented in the Genesys platform by Digilent, Inc. [26], based on a Xilinx Virtex5 LX-50T FPGA [27]. For this experimental approach, the global parameters of the design have been defined according to Table 1. This allows a frequency of $f_{mclk} = 100$ MHz for the master clock. The resource consumption of the design can be seen in Table 2 for the aforementioned FPGA device, not only for the peripheral core, but also for the global system including the MicroBlaze module.

Table 3 shows the datawidth defined for each parameter in the design. These values have been configured as a trade-off between fixed-point representation errors and resource consumption. The FPGA design has been validated by means of post-place-route simulation.

Table 1
Global parameter definition for experimental implementation.

Parameter	Symbol	Value
Global clock frequency	f_{mclk}	100 MHz
Sampling frequency	f_S	390.625 kHz
Number of beacons	I	5
Number of Doppler frequencies	K	7
Interpolation factor	Q	512
Oversampling	M	10
Kasami code length	L	255

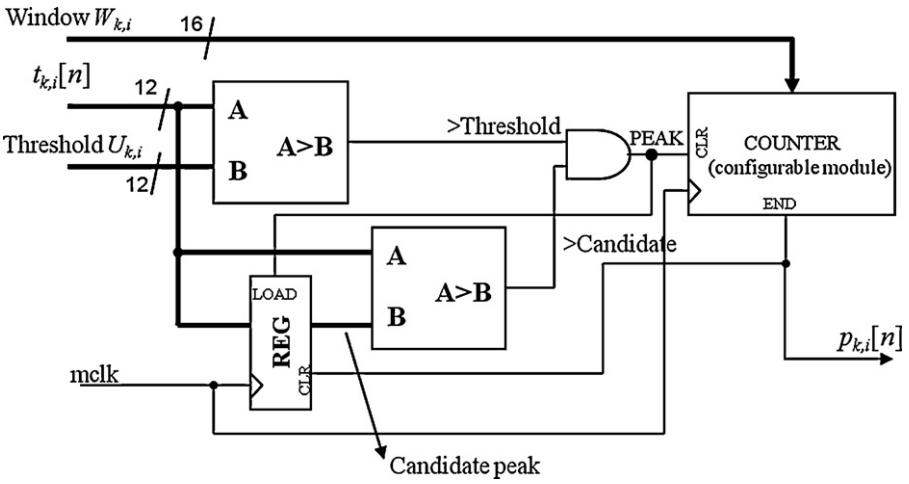

Fig. 14. Block diagram of the peak detector proposed for detection of beacon transmissions.

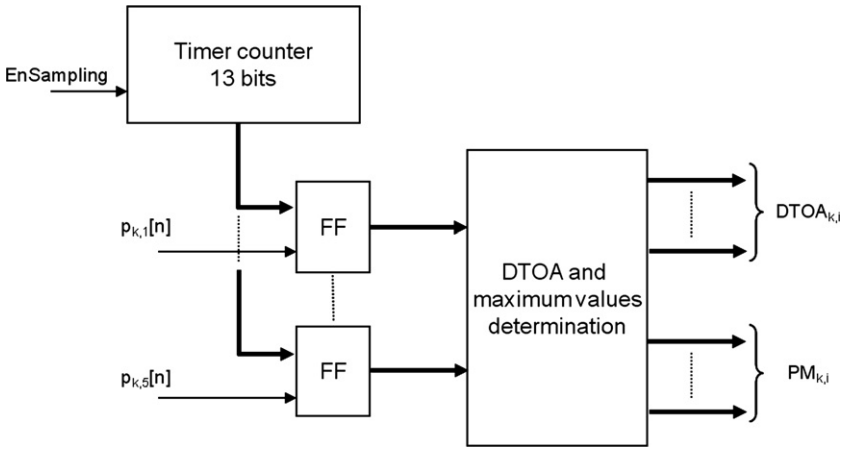

Fig. 15. Block diagram of the DTOA determination module.

5.1. Synthetic signals analysis

The performance of the Doppler-tolerant receiver was first statistically analysed by modelling the signals that would reach this system in 25 different locations, uniformly distributed in a horizontal grid of 4 m × 4 m placed at 1 m high. For each one of these locations, 8 different velocity directions have been considered in a horizontal plane with angular increments of $2\pi/8$ rads among them. Fig. 16 shows the cumulative error in DTOAs determination for all beacons, considering three different velocity magnitudes of 0.5, 1.5 and 3 m/s and assuming SNR = 0 dB. The performance of the classic and the Doppler-tolerant receiver are represented in the left and right columns of this figure respectively. As can be seen, the behaviour of both detectors is similar with low velocity magnitudes, but when this value increases above 1 m/s, the percentage of detection of the classic receiver clearly decreases below 100%. In the Doppler-tolerant receiver, 100% of the DTOAs measurements exhibit an error below 18 μs (6.18 mm at 20 °C) even with receiver speeds as large as 3 m/s.

The cumulative error in radial speed estimation has also been analysed by using the same set of synthetically generated signals, but considering in this case 6 different velocity magnitudes ranging from 0.5 m/s to 3 m/s in increments of 0.5 m/s, for a total of 1200 different test situations. Fig. 17 shows this cumulative error for all beacons and three different values of SNR = 0, −3 and −6 dBs. Also, taking into account that according to Eq. (18) the estimated speeds depend on the values measured for the magnitude of the correlation peaks, this figure compares the errors that would be generated by a floating-point processor against the actual errors generated by the fixed-point architecture described in Table 3. As can be seen, there is little deterioration in the cumulative error curves with decreasing values of SNR, and there are no significant differences between the results obtained with the floating-point and fixed-point precisions.

Table 2
Resource consumption in Xilinx Virtex5 LX-50T FPGA of the global design.

Resource	IP core		Global system	
	No.	Percentage (%)	No.	Percentage (%)
Slices	6290	87.36	6952	96.56
RAMB16	11	18.33	18	30.00
DSP48	7	12.07	10	17.24

Table 3
Datawidth definition for the parameters of the design.

Signal	Parameter	Number of bits
Acquired signal	$r[n]$	12
Interpolated signal	$r_p[n]$	8
Doppler input signal	$r_k[n]$	8
Demodulation signal	$d_k[n]$	8
Correlation signal	$t_{k,i}[n]$	20
Correlation maximum values	$PM_{k,i}[n]$	12
Difference in Time-Of-Flight	$DTOA_{k,i}$	13

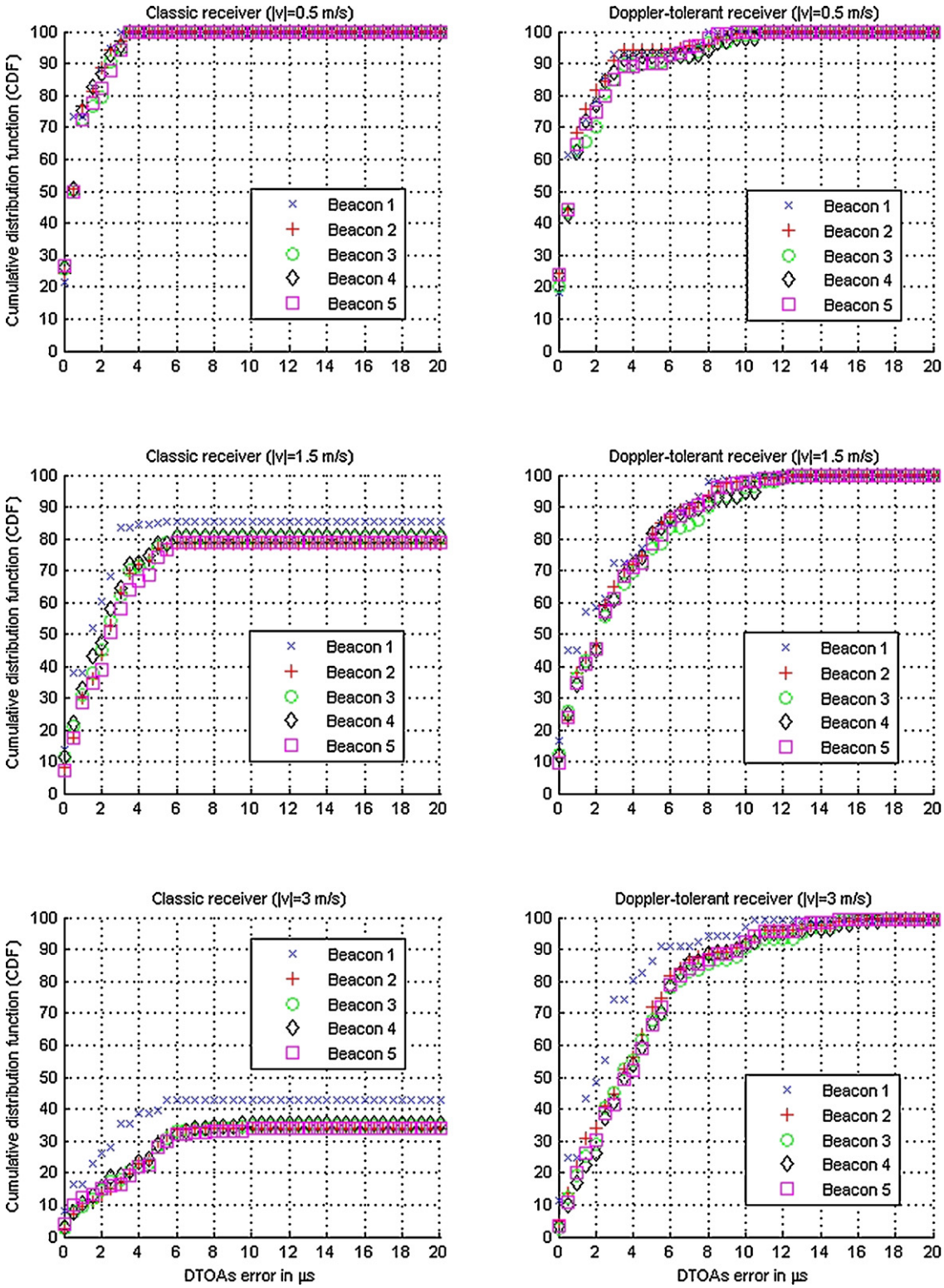

Fig. 16. Cumulative error in DTOAs determination for three different velocity magnitudes in the classic receiver (left column) and the Doppler-tolerant receiver (right column). In all cases SNR = 0 dB was assumed. Non-detections are included as infinite-error detections.

5.2. Real signals analysis

The signals used in the previous section to analyse system performance were modelled considering generic phenomena such as the atmospheric absorption of ultrasonic waves in air and the presence of Gaussian additive noise in the received signal. However, there are other phenomena, depending on the particular features of the uLPS infrastructure where the receiver is used, that may significantly degrade the results shown in Figs. 16 and 17. Among them, there are the non-ideal response of the ultrasonic beacons, the presence of different sources of noise and, most importantly, multi-path propagation effects. For this reason, the performance of

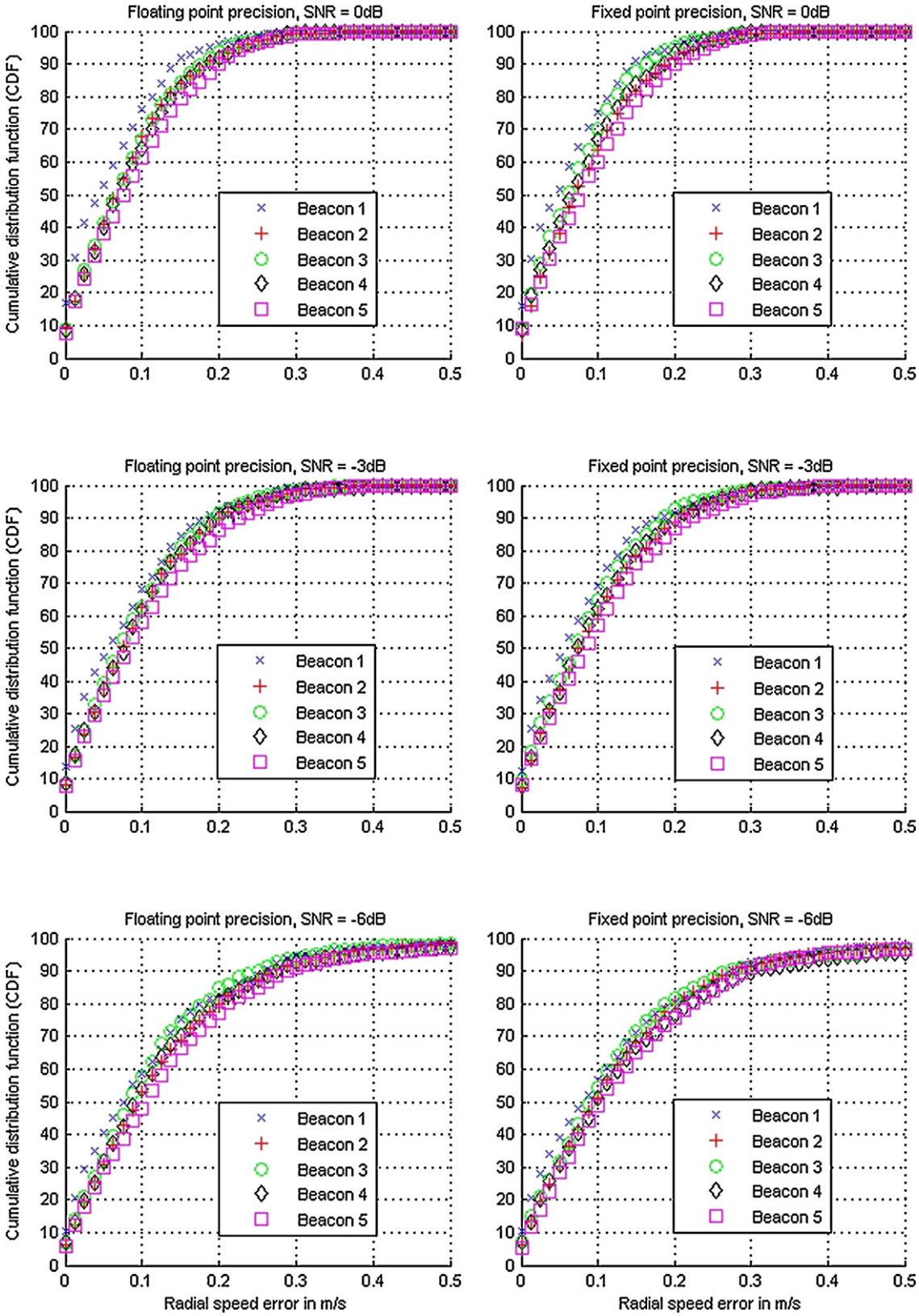

Fig. 17. Cumulative error in radial speeds estimates for different values of SNR considering floating-point precision (left column) and the actual fixed-point precision (right column).

the Doppler-tolerant receiver was also analysed with real signals generated by the uLPS infrastructure described in Section 2.

Because of the reduced dimensions of the room where this system is currently installed, and in order to cover a wide range of controlled speeds in different locations, a Pioneer 3DX mobile robot with a 1.98 m long bar installed in its top platform has been used to host the receiver. This robot was placed close to the origin of coordinates (see Fig. 1(a)) and it was programmed to rotate at

Fig. 18. Pioneer 3DX robot with the ultrasonic microphone attached at the end of the bar used to capture real signals at different speeds.

different angular speeds ranging from 0.5 to 3.5 rad/s, corresponding to receiver linear velocities from 0.98 to 6.82 m/s when this receiver is installed at the bar's end. Fig. 18 shows the robot with the horizontal bar and the ultrasonic microphone at the end of this bar. The laptop's screen displays the ultrasonic signals received at that moment, with a new emission from all beacons every 60 ms.

Fig. 19 shows the cumulative error in DTOAs determination for all beacons, considering two different angular velocities of 0.5 and 3.5 rad/s, both for the classic receiver (left column) and for the Doppler-tolerant receiver (right column). It is important to note that these results were derived from the anaysis of the signals acquired along a circumference of radius 1.98 m centered close to the origin of coordinates. This fact explains the good results obtained for beacon 1, even with the classic receiver at high angular speed, since the radial speed of the receiver with respect to this beacon is always very small for this particular trajectory. Also, note that the worst results were always obtained for beacon 5. After analysing these results, we independently measured the Sound Pressure Level (SPL) of all beacons and detected an unusually low value of this parameter for beacon 5, that we have attributed to a manufacturing defect.

Degraded system performance caused by the above mentioned real phenomena becomes evident if we notice that the 100% detection percentage is no longer achieved even at very low speeds, and also that the maximum error represented in this figure is four times that represented in Fig. 16. This significant increment of the error may also be explained by the fact that it is difficult to accurately establish the real position of the receiver while the robot is turning,

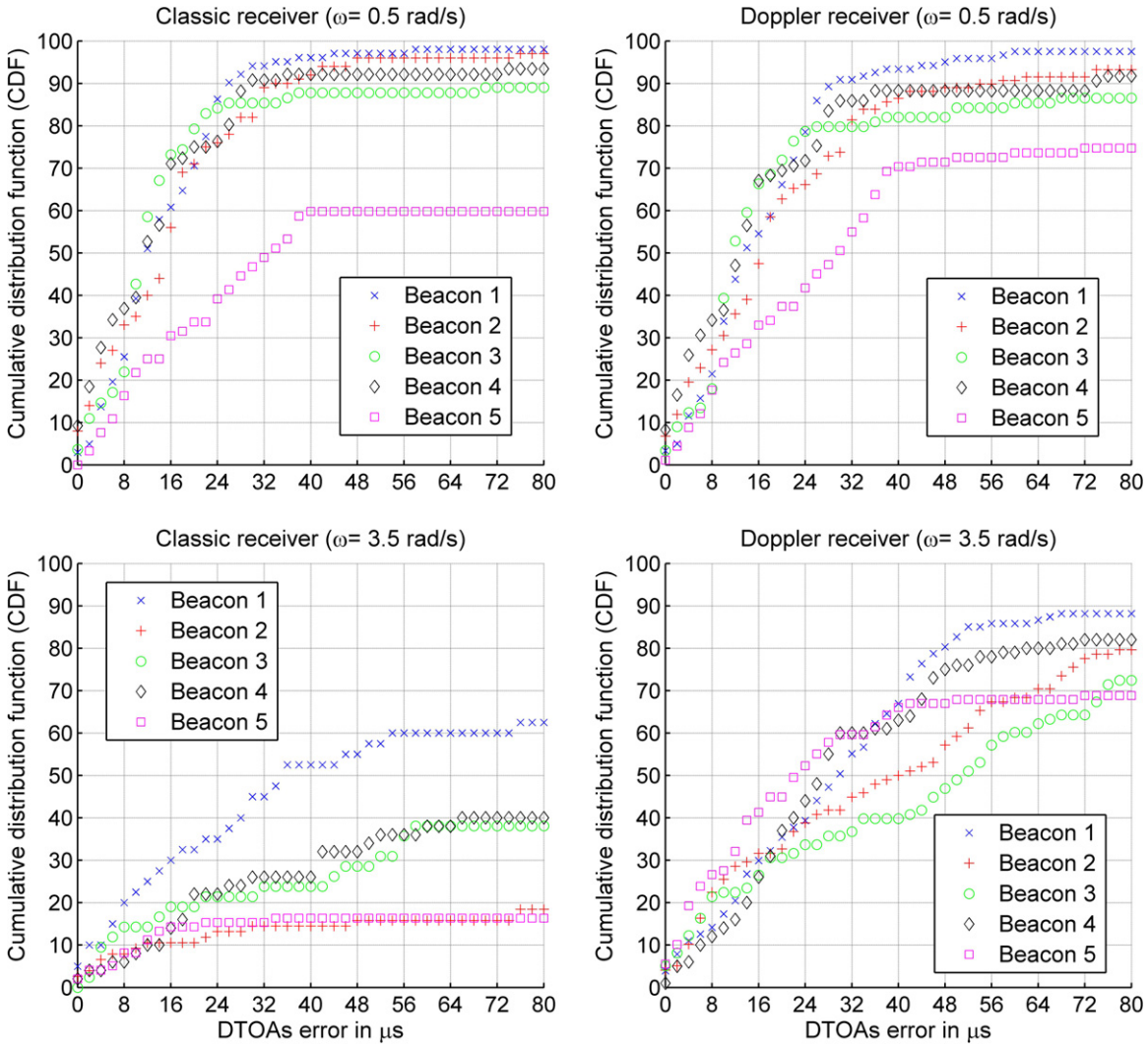

Fig. 19. Cumulative error in DTOAs determination for two different angular speeds in the classic receiver (left column) and in the Doppler-tolerant receiver (right column). Non-detections are included as infinite-error detections.

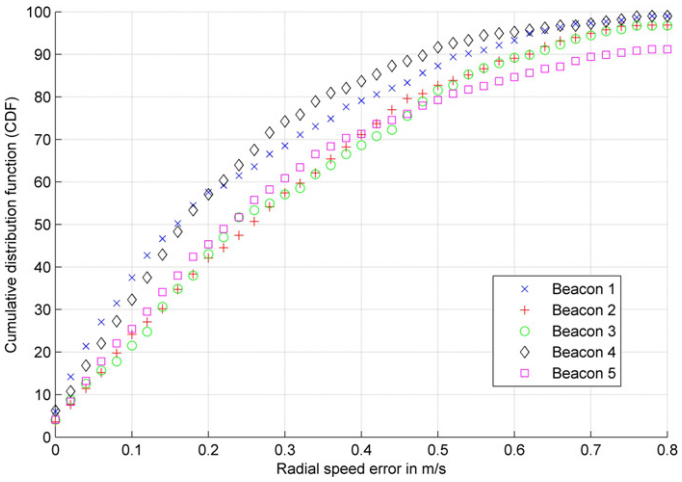

Fig. 20. Cumulative error in radial speeds estimates for all beacons.

since this movement makes the robot slip slightly out of its original position. In any case, this figure confirms that the percentage of detection of the Doppler-tolerant receiver supersedes that of the classic receiver with high receiver speeds in most cases.

Finally, Fig. 20 shows the cumulative error in radial speed estimation for all beacons when turning the robot at seven different angular speeds from 0.5 to 3.5 rad/s in increments of 0.5 rad/s. As can be seen in this figure, 90% of data from all beacons fall below an error of 0.8 m/s in radial speed estimation. Again, the best results are obtained from beacon 1 and the worst from beacon 5 for the same reasons explained above.

6. Conclusions

This work has presented a novel Doppler-tolerant receiver for a broadband ultrasonic Local Positioning System. The main element of this receiver is a set of seven banks of 5 Kasami correlators, each one matched to a different frequency-shifted version of the codes to be detected. These banks are identical in practice, since the frequency-shift matching is obtained by means of a multirate filter bank that compensates for the Doppler effect of the incoming signal. The interpolation factor Q determines the Doppler resolution of the detector, that is 0.67 m/s in our system ($Q = 512$).

The whole system has been implemented in a Virtex-5 FPGA-based platform working at a master clock frequency of 100 MHz. The hardware implementation of every stage in the system, including the interpolation module, the dispatcher, the BPSK demodulator, the Kasami correlators, the peak detector and the DTOA determination module, has been described in detail and validated by means of a post-place-route simulation. All these stages, together with a bank of communication registers, constitute a complex peripheral which is accessed by a Microblaze processor via PLB bus.

The performance of the receiver has been first analysed with a set of 1200 test signals synthetically generated to simulate different positions and velocities for this receiver. The results show that the sensor is capable of detecting the signals coming from all the beacons when moving at velocities of up to 3 m/s in a horizontal plane of 4 m × 4 m and with very low values of SNR. These simulated results also show that the largest errors in DTOA determination are approximately of 18 μs.

The system performance has been also analysed with signals generated by a real uLPS infrastructure, the aim being to study the impact that phenomena depending on a particular architecture, such as transducers response or the multipath propagation effect, may have on performance. Real results clearly show the relevance of these phenomena, since 100% detection percentage is no longer achieved even with very low receiver velocities. Also, the maximum error in DTOAs determination is increased by a factor of ≃4. Real data analysis confirms the improved capability of the proposed Doppler-tolerant receiver to detect high bandwidth ultrasonic signals from a moving receiver.

Finally, we would like to remark that in the proposed sensor the Microblaze processor has been used to calculate the DTOA of the signals coming from all the beacons, to estimate the receiver radial speed with respect to these beacons and to communicate these data to a central computer via a RS-232 port, where they are visualized and further processed. Nevertheless, the hyperbolic trilateration algorithms used to estimate the receiver location from the measured DTOAs could be programmed into the Microblaze, fully exploiting the resources of this processor to design a sensor that would not need the participation of an external processing unit.

Acknowledgements

This work was supported by the Spanish Ministry of Science and Innovation (LEMUR project, Ref. TIN2009-14114-C04-01/04), the University of Alcalá (FUVA project, Ref. CCG10-UAH/TIC-5988), and the Regional Goverment of Extremadura through the European Regional Development Funds (GR10097).

References

[1] M. Addlesee, R. Curwen, S. Hodges, J. Newmann, P. Steggles, A. Ward, A. Hopper, Implementing a sentient computing system, IEEE Computer 34 (8) (2001) 50–56.
[2] C. Randell, H. Muller, Low cost indoor positioning system, in: Proceedings of the 3rd International Conference on Ubiquitous Computing, Atlanta, USA, 2001, pp. 42–48.
[3] M. Hazas, A. Ward, A novel broadband ultrasonic location system, in: Proceedings of the 4th International Conference on Ubiquitous Computing (UbiComp 2002), Göteborg, Sweden, 2002, pp. 264–280.
[4] M. Hazas, A. Ward, A high performance privacy-oriented location system, in: Proceedings of the 1st IEEE International Conference on Pervasive Computing and Communications (PerCom 2003), Dallas, USA, 2003, pp. 216–223.
[5] J. Ureña, A. Hernández, J.M. Villadangos, M. Mazo, J.C. García, J.J. García, F.J. Álvarez, C. de Marziani, M.C. Pérez, J.A. Jiménez, A. Jiménez, F. Seco, Advanced sensorial system for an acoustic LPS, Microprocessors and Microsystems 31 (2007) 393–401.
[6] M.C. Pérez, J. Ureña, A. Hernández, A. Jiménez, D. Ruíz, C. de Marziani, F.J. Álvarez, Efficient hardware implementation for detecting CSS-based loosely synchronous codes in a local positioning system, in: Proceedings of the 2009 IEEE Conference on Emerging Technologies and Factory Automation, Mallorca, Spain, 2009.
[7] J.R. González, C.J. Bleakley, High-precision robust broadband ultrasonic location and orientation estimation, IEEE Journal of selected topics in Signal Processing 3 (5) (2009) 832–844.
[8] J. Werb, C. Lanzl, Designing a positioning system for finding things and people indoors, IEEE Spectrum 35 (9) (1998) 71–78.
[9] K. Whitehouse, C. Karlof, D. Culler, A practical evaluation of radio signal strength for ranging-based localization, ACM SIGMOBILE Mobile Computing and Communications Review 11 (1) (2007) 41–52.
[10] K. Arshak, F. Adepoju, A model for estimating the real-time positions of a moving object in wireless telemetry applications using RF sensors, in: Proceedings of the IEEE Sensors Applications Symposium, San Diego, USA, 2007, pp. 1–6.
[11] S. Tilch, R. Mautz, Current investigations at the ETH Zurich in optical indoor positioning, in: Proceedings of the 7th Workshop on Positioning Navigation and Communication, Dresden, Germany, 2010, pp. 174–178.
[12] V. Willert, Optical indoor positioning using a camera phone, in: Proceedings of the 2010 International Conference on Indoor Positioning and Indoor Navigation (IPIN 2010), Zürich, Switzerland, 2010.
[13] J. Blankenbach, A. Norrdine, H. Hellmers, Adaptive signal processing for a magnetic indoor positioning system, in: Proceedings of the 2011 International Conference on Indoor Positioning and Indoor Navigation (IPIN 2011), Guimarães, Portugal, 2011.
[14] S. Holm, O.B. Hovind, S. Rostad, R. Holm, Indoors data communications using airborne ultrasound, in: Proceedings of the IEEE Int. Conf. Acoustics, Speech, Sign. Proc, Philadelphia, PA, USA, 2005, pp. 957–960.
[15] M. Alloulah, M. Hazas, An efficient CDMA core for indoor acoustic position sensing, in: Proceedings of the 2010 International Conference on Indoor Positioning and Indoor Navigation (IPIN), Zürich, Switzerland, 2010.

[16] J.A. Paredes, T. Aguilera, F.J. Álvarez, J. Lozano, J. Morera, Analysis of Doppler effect on the pulse compression of different codes emitted by an ultrasonic LPS, Sensors 11 (2011) 10765–10784.
[17] M. McCarthy, H. L. Muller, Positioning with independent ultrasonic beacons, Tech. Rep. CSTR-05-005, Department of Computer Science, University of Bristol (September 1995).
[18] H.L. Muller, M. McCarthy, C. Randell, Particle filters for position sensing with asynchronous ultrasonic beacons, in: Proceedings of the 2nd International Conference on Location and Context Awareness, Dublin, Ireland, 2006, pp. 1–13.
[19] J. Villadangos, J. Ureña, M. Mazo, A. Hernández, C.D. Marziani, M.C. Pérez, F.J. Álvarez, J.J. García, A. Jiménez, I. Gude, Ultrasonic local positioning systems with large covered area, in: Proceedings of the 2007 International Symposium on Intelligent Signal Processing (WISP'07), Alcalá de Henares, Spain, 2007.
[20] Xilinx, Spartan-3E FPGA Family Complete Datasheet, product specification (April 2008).
[21] T. Kasami, Weight distribution formula for some class of cyclic codes, Tech. Rep. R-285, Coordinated Science Lab, University of Illinois (1966).
[22] H. Peremans, K. Audenaert, J.V. Campenhout, A high resolution sensor based on tri-aural perception, IEEE Transactions on Robotics and Automation 9 (1) (1993) 36–48.
[23] F.J. Álvarez, J. Ureña, M. Mazo, A. Hernández, J.J. García, C.D. Marziani, High reliability outdoor sonar prototype based on efficient signal coding, IEEE Transactions on Ultrasonics, Ferroelectrics and Frequency Control 53 (10) (2006) 1862–1871.
[24] M.C. Pérez, J. Ureña, A. Hernández, F.J. Álvarez, W.P. Marnane, Efficient real-time correlator for LS sequences, in: Proceedings of the IEEE International Symposium on Industrial Electronics (ISIE 2007), Vigo, Spain, 2007, pp. 1663–1668.
[25] A. Hernández, J. Ureña, J. García, M. Mazo, D. Herranz, J. Dérutin, J. Sérot, Ultrasonic ranging sensor using simultaneous emissions from different transducers, IEEE Transactions on Ultrasonics, Ferroelectrics and Frequency Control (12) (2004) 1660–1670.
[26] Inc. Digilent, Genesys Board Reference Manual, Product Specification, 2012.
[27] Xilinx, Inc., Virtex-5 Family Overview, Product Specification, 2009.

Biographies

Fernando J. Álvarez received his Physics degree from the University of Sevilla (Spain) in 1998 and his PhD degree in Electronics from the University of Alcalá (Spain) in 2006. He is currently an Associate Professor of Digital Electronics in the Department of Electrical Engineering, Electronics and Automatics at the University of Extremadura, Spain, where he is also the head of the Sensory Systems Group. His research areas of interest include local positioning systems, ultrasonic signal processing and outdoor acoustics.

Álvaro Hernández obtained his PhD from the University of Alcalá (Spain), and from the Blaise Pascal University (France) in 2003. He is currently an Associate Professor of Digital Systems and Electronic Design at the Electronics Department in the University of Alcalá. His research areas are multi-sensor integration, electronic systems for mobile robots, digital and embedded systems.

José A. Moreno received his Computer Engineering degree from the University of Deusto (Spain) in 1993. He is currently an Associate Professor of Digital Systems and Microprocessors in the Department of Electrical Engineering, Electronics and Automatics at the University of Extremadura, Spain. His research areas of interest include reconfigurable computing, embedded computing and digital signal processing systems.

M. Carmen Pérez received the MS degree in electronics engineering and the PhD degree from the University of Alcalá (UAH), Spain in 2004 and 2009, respectively. She is currently an Assistant Professor at the Electronics Department of the University of Alcalá. Since 2003 she has collaborated on several research projects in the areas of sequence design, low-level ultrasonic signal processing and computing architecture.

Jesús Ureña received the B.S. degree in Electronics Engineering and the M.S. degree in Telecommunications Engineering from the Polytechnical University of Madrid, Spain, in 1986 and 1992, respectively; and the Ph.D. degree in Telecommunications from the University of Alcalá, Spain, in 1998. Since 1986, he has been with the Department of Electronics, University of Alcalá, currently as a Full Professor. During the period 1993–1997 he was the head of the Department. He has collaborated in several educational and research projects in the area of electronic control and sensory systems for mobile robots and wheelchairs and in the area of electronic distributed systems for railways. His current research interests are in the areas of low-level ultrasonic signal processing, local positioning systems, and sensory systems for railway safety.

Carlos De Marziani obtained his Electronics Engineering degree from the University of Patagonia San Juan Bosco (Argentina) in 2001. In 2007, he obtained his PhD at the Electronics Department from the University of Alcalá (Spain). He is currently Professor of Digital Systems at the Electronics Department from the University of Patagonia San Juan Bosco and also Assistant Researcher of National Council on Scientific and Technical Research, Argentina (Consejo Nacional de Investigaciones Científicas y Técnicas, CONICET). His research areas are sensor networks, multi-sensor integration, electronic systems for mobile robots and digital systems.